Journal of Power Sources, 38 (1992) 87–102

Conversion of tetrabasic lead sulfate to lead dioxide in lead/acid battery plates

L. T. Lam, A. M. Vecchio-Sadus, H. Ozgun and D. A. J. Rand
CSIRO, Division of Mineral Products, P.O. Box 124, Port Melbourne, Vic. 3207 (Australia)

Abstract

The formation of cured lead/acid battery plates containing a high level (~70 wt.%) of tetrabasic lead sulfate ($4PbO \cdot PbSO_4 = 4BS$) has been studied under both cyclic voltammetric and constant-potential conditions. The resulting phase composition is determined by an X-ray diffraction technique, while the morphology is examined by both optical and scanning-electron microscopy. The cyclic voltammogram for a 4BS cured plate displays only one anodic peak in the 'PbO_2' region. X-ray diffraction phase-analysis confirms that this is due to the conversion of $PbSO_4$ to the β polymorph of PbO_2. Thus, the long-held belief that 4BS promotes the formation of α-PbO_2 is shown to be incorrect. The formation process commences at the grid surface and then spreads into the cured material, preferentially via the surface of the 4BS crystalline network. The product consists of a large number of fine β-PbO_2 particles gathered into porous agglomerates that retain the overall geometry of the 4BS network. The dioxide morphology can vary widely — from laminar to anhedral shapes — and is determined largely by the value of the applied potential. Thus, the industrial practice of conducting formation under constant-current (as opposed to constant-potential) conditions may result in plates with inconsistent physicochemical characteristics.

Introduction

Two crystal modifications of lead dioxide are found in the positive-plate active material of lead/acid batteries, namely, α-PbO_2 (orthorhombic) and β-PbO_2 (tetragonal). Although these two polymorphs differ in structure only by the arrangement of the oxygen octahedra, there are marked differences in the respective physical properties (Table 1). The reported data vary appreciably between investigators, but it is generally claimed that, compared with β-PbO_2, α-PbO_2 has a more compact morphology, greater mechanical strength, larger pore/crystallite size and higher conductivity, but lower surface area and less discharge capacity. Moreover, it has been found [7] that there is a difference in the discharge behaviour of the two polymorphs: α-PbO_2 does not follow completely the 'double sulfate theory' for lead/acid batteries with the result that PbO and basic lead sulfates, rather than $PbSO_4$, are produced during discharge to below 0 V versus Hg/Hg_2SO_4.

The α form of PbO_2 is deposited electrochemically in a neutral or alkaline environment, the β form in an acidic environment. The distribution of the two polymorphs in positive battery plates has been examined by various authors [6, 8–14]. These studies have revealed that whereas β-PbO_2 predominates in outer surface layers of the plates, α-PbO_2 resides in the inner zones. This finding suggests that a pH gradient develops within the active material during plate formation [12, 15–18]. Ikari *et al.* [19] have

0378-7753/92/$5.00

TABLE 1

Physical and electrical characteristics of α- and β-PbO_2

Parameters	α-PbO_2	β-PbO_2	Reference
Density (g cm^{-3})	9.1–9.4	9.1–9.4	1
Pore size (nm)	<60	<10	2
Crystallite size (nm)	55	20	2
BET surface area (m^2 g^{-1})	0.48	9.53	3
Discharge capacity (A h g^{-1})	0.041	0.113	4
	0.110	0.172	5
	0.135	0.164	6

shown that a high pH can be created through the transport of acid to the interior of plates becoming restricted under the influence of various factors including: coverage of the plate surface with a dense film of lead sulfate; a dilute electrolyte; a high PbO content in the cured material; a high paste density.

Attempts have also been made to detect relationships between the phase compositions of plates in the cured and formed states. The findings have given rise to the 'tetrabasic lead sulfate → α-PbO_2' debate (for a review see ref. 20). Large, square-prismatic crystals of tetrabasic lead sulfate ($4PbO \cdot PbSO_4 = 4BS$) are produced in pasted plates when curing is conducted under conditions of high temperature and high relative humidity (i.e., ~80 °C/100% r.h.). It is considered that these crystals interlock to produce a reticular structure that increases the mechanical strength of the active material. Other studies [21] have indicated that the large number of fine PbO_2 crystals produced during the subsequent formation stage gather into porous agglomerates that retain the shape of the precursor 4BS crystal skeleton via a metasomatic process [22–25]. Finally, it has been argued [16, 26, 27] that the reticular structure in the formed plate is composed of α-PbO_2. Thus, it has become commonplace to accept that 4BS favours the formation of α-PbO_2 (and, by analogy, that tribasic lead sulfate ($3PbO \cdot PbSO_4 \cdot H_2O = 3BS$) yields β-PbO_2). In reviewing the role of 4BS in lead/acid positive plates, however, Culpin [20] demonstrated that the preponderance of experimental evidence refutes such a conclusion — the identity of PbO_2 resulting from the conversion of 4BS (or 3BS) is in fact influenced by the complex interplay of a wide range of parameters including: paste composition and density; plate thickness; acid specific gravity; temperature.

This study has used the investigative techniques of cyclic voltammetry and X-ray diffraction phase-analysis to characterize the phase chemistry of the oxidation product derived from 4BS during the formation of cured positive-plate material. The change in morphology of the product obtained at various constant potentials has been examined by both optical and scanning electron microscopy. Experiments have been conducted in excess acid in order to suppress the influence of any pH gradient (generated by other plate/cell design factors) on the nature of the oxidation product.

Experimental

Sample preparation

Positive-plate paste with a density of 4.0 to 4.1 g cm^{-3} was prepared from leady oxide, sulfuric acid solution and water using the formulation and mixing conditions

TABLE 2

Paste formulation for positive-plate material

Leady oxide[a] (g)	1000
Carboxymethyl cellulose (g)	1.1
Water (cm^3)	130
1.4 sp. gr. H_2SO_4	93
Mixing time (min)	10–12
Final mix (min)	1
Paste density (g cm^{-3})	4.0–4.1

[a]Leady oxide: 24 wt.% Pb; 64 wt.% α-PbO; 12 wt.% β-PbO; (Barton-pot variety).

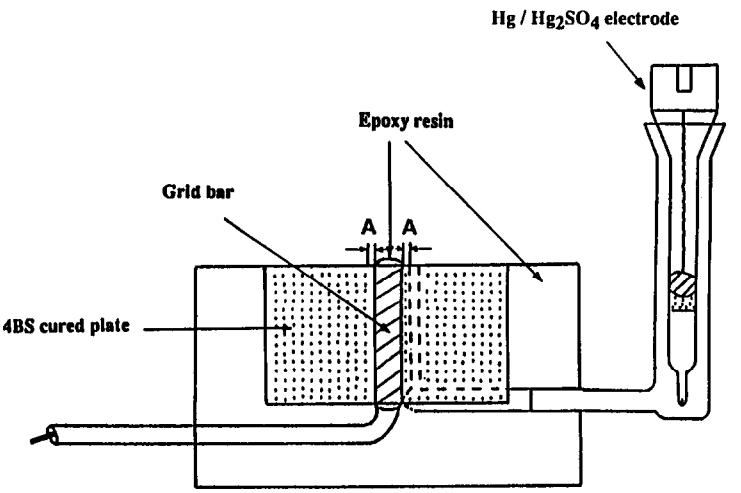

Fig. 1. Schematic of working electrode assembly.

given in Table 2. The paste was applied, by hand, to a Pb–5wt.%Sb grid (5 mm thick) and then compacted under the weight (5 kg) of a specially made stainless-steel roller. After pasting, the plate was mounted vertically in a stainless-steel rack and placed in a petri dish that contained a small amount of distilled water. The complete assembly was enclosed in a sealed plastic bag.

Curing was conducted for 48 h in an oven maintained at 90 °C and 100% r.h. The high humidity was achieved by evaporation of the distilled water. After curing, the plate was removed, dried at 90 °C for a further 3 h, and then allowed to return to room temperature in a desiccator that contained silica to keep the moisture level of the surrounding atmosphere at a low level.

One-fourth of the cured positive plate was removed and impregnated with epoxy resin under vacuum in a desiccator. After setting, a small section (20×20 mm) was cut from the middle of the sample in order to avoid any influence of the shearing force on the intrinsic contact between the active material and the grid members. A copper wire was soldered to a grid bar that had become exposed in the cross section of the excised sample. The assembly was re-embedded in epoxy resin to give a cylinder of diameter = 30 mm and hight = 30 mm. After setting, holes were drilled into both the side and top of the mould to allow the connection of a small Hg/Hg_2SO_4 reference

electrode via a Luggin capillary (Fig. 1). The upper surface of the mould was polished with abrasive papers of successively finer grades between 240 and 1200 grit. Final polishing was conducted on cloths impregnated, in turn, with alumina slurries of decreasing particle size, namely, 20, 5, 1 and 0.5 μm.

Plate formation

After polishing, the Hg/Hg_2SO_4 reference electrode was attached to the sample. The entire block was immersed in a dish containing 1.05 sp.gr. H_2SO_4 and then placed under an optical stereoscopic microscope (Nikon SMZ-2T). A lead sheet was used as a counter electrode. The potential of the sample was scanned with a programmable potentiostat/galvanostat (EG&G PAR 273) and the resulting voltammograms were recorded on an X-Y recorder (Bryans 26000 A3). In another series of experiments, plate formation was carried out at different constant potentials and the subsequent changes in both surface composition and morphology were photographed with a

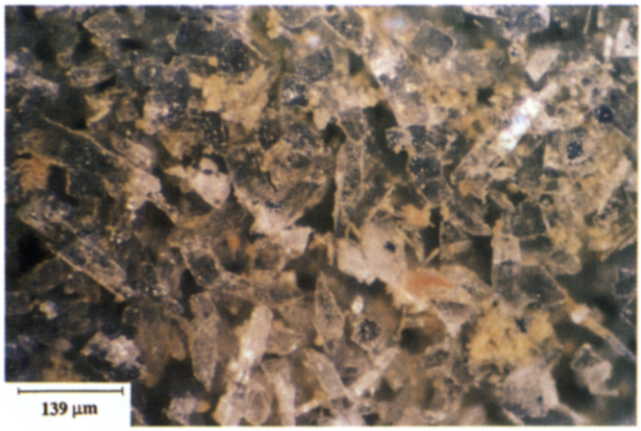

(a)

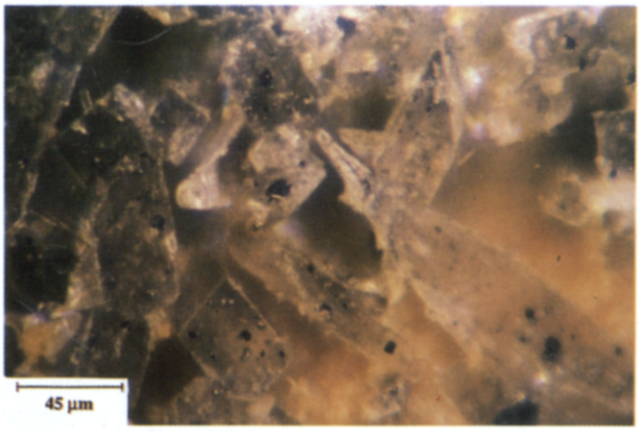

(b)

Fig. 2. Optical micrographs of cross section of 4BS cured material. Magnification: (a) ×99; (b) ×300.

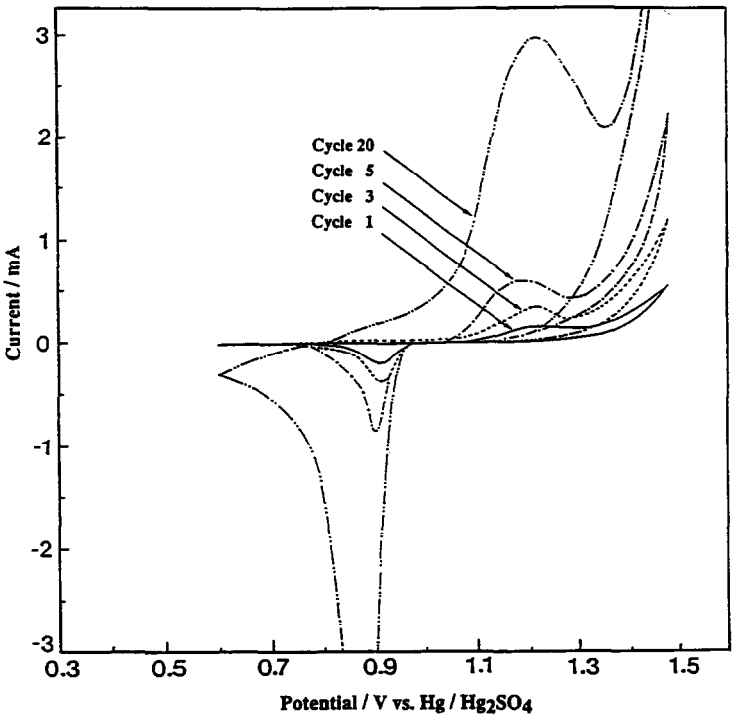

Fig. 3. Cyclic voltammograms for 4BS cured material in 1.05 sp. gr. H_2SO_4.

35 mm camera (Olympus OM-2N) that was attached to the optical microscope. All experiments were performed at room temperature (18 to 20 °C) and all potentials are reported with respect to a Hg/Hg_2SO_4, 5 M H_2SO_4 reference electrode.

X-ray diffraction phase-analysis

Samples of leady oxide, paste and cured/formed materials were subjected to X-ray diffraction (XRD) phase-analysis. X-ray peak intensities were obtained (applying an automated, integrated, step-scan procedure) on a standard Philips PW1710 diffractometer fitted with a curved graphite monochromator using copper Kα radiation. The data were collected on chart paper (for visual examination) and also stored on computer files (for subsequent computational analysis). The phase compositions were determined by PEAKS® — an advanced XRD method developed in the CSIRO laboratories [28]. The latter uses measurements of the peak height to determine quantitatively the relative amounts of the individual crystalline phases.

Scanning electron microscopy

The morphology of the formed plate material was examined with a JEOL JSM-25S III scanning electron microscope. A sample of formed material (~1 mm thick) was mounted on a carbon block and a gold–palladium coating was deposited over the entire block to provide satisfactory imaging of the material.

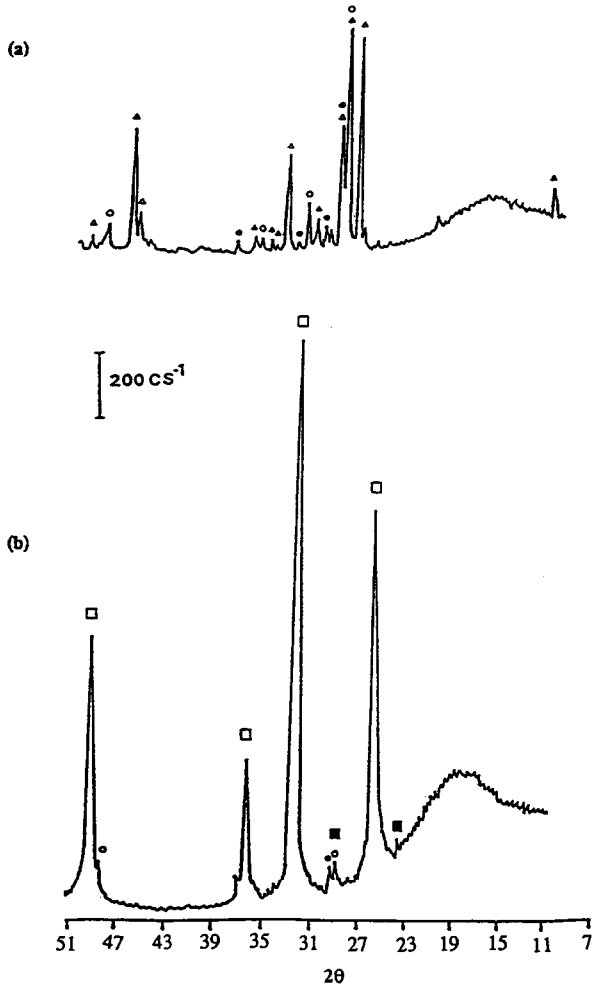

Fig. 4. X-ray diffraction patterns for: (a) 4BS cured material; (b) material formed at 1.2 V. (△) 4BS; (○) α-PbO; (●) β-PbO; (▲) Pb; (■) α-PbO_2; (□) β-PbO_2.

Results and discussion

Phase composition/morphology of 4BS cured material

As mentioned above, 4BS cured material is produced under high-temperature/high-r.h. conditions. The yield of 4BS is determined by the acid-to-leady oxide ratio involved in the paste formulation. For example, it has been claimed [29] that the maximum 4BS content is achieved when the ratio is between 4 and 6%. Phase-analysis showed that the cured material prepared in this study comprised: 73 wt.% 4BS; 21 wt.% α-PbO; 4 wt.% β-PbO; 2 wt.% Pb. (Note, the acid-to-oxide ratio in the paste was 6.5%.)

After curing, the plate had an orange-coloured surface and a dark-green interior. Optical micrographs (Fig. 2) revealed that the latter consisted of large, transparent, square-prismatic 4BS crystals with lengths up to hundreds of microns.

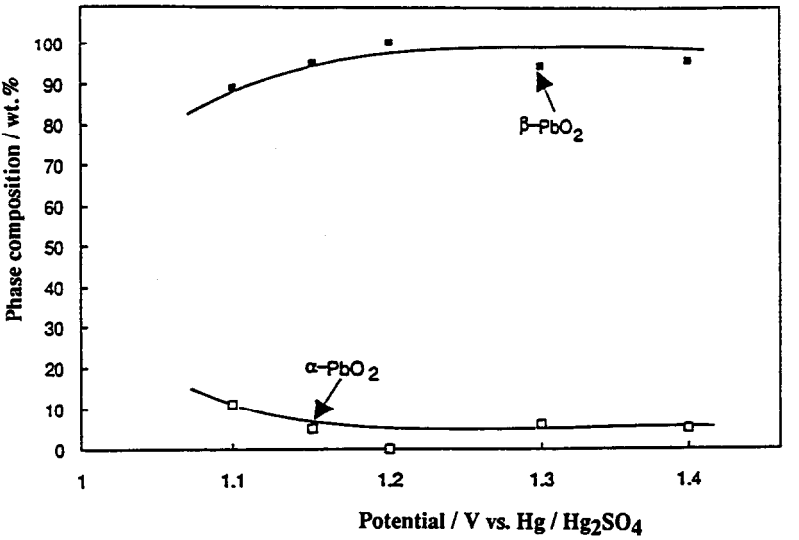

Fig. 5. Change in phase composition of formed active material with applied potential.

Oxidation of 4BS cured material

Other workers have studied the cyclic-voltammetric characteristics of lead [30–32] and lead–calcium alloys [33] in sulfuric acid solutions. By comparison, surprisingly little attention has been paid to the corresponding behaviour of lead–antimony alloys. For the former two systems, potential scanning in the range 0 to 1.6 V results, on the second cycle, in the development of an anodic peak (P_2) at ~1.4 V prior to oxygen evolution. With further cycling, P_2 increases in size and a second peak (P_1) appears at a more negative potential, namely, 1.05 V. Peaks P_1 and P_2 have been assigned to the growth of α-PbO_2 and β-PbO_2, respectively: the former by oxidation of PbO and basic lead sulfates (brought about by pH changes beneath the $PbSO_4$ film [17, 18]), and the latter by oxidation of $PbSO_4$. To date, no definitive experimental evidence has been obtained to verify this hypothesis.

In this study, the Pb–Sb grid alloy was prevented from influencing, or contributing to, the features of the voltammograms by covering the upper, exposed section (Fig. 1) with epoxy resin. The potential of the sample was held initially at 1.5 V in 1.05 sp. gr. H_2SO_4 for 20 min until the cured material adjacent to the encapsulated grid (regions A, Fig. 1) became converted to PbO_2. This provided the necessary conductive pathway for subsequent voltammetric studies. The potential of the sample was scanned between 0.6 and 1.5 V at 0.5 mV s^{-1}; the resulting voltammograms are given in Fig. 3. It can be seen that there is only one anodic peak at ~1.2 V and one cathodic peak at ~0.89 V. These two peaks increase with repetitive cycling and are similar to those attributed by the above authors to the formation of β-PbO_2 and its subsequent reduction to $PbSO_4$.

In a second series of experiments, the sample was held at different constant potentials between 1.1 and 1.4 V, i.e., over the region where the 'β-PbO_2' peak appeared in Fig. 3. Each potential was applied until the entire surface of the sample was converted to the oxidation product; the periods required to complete the individual experiments ranged from 1 to 3 weeks. After oxidation, each sample was removed,

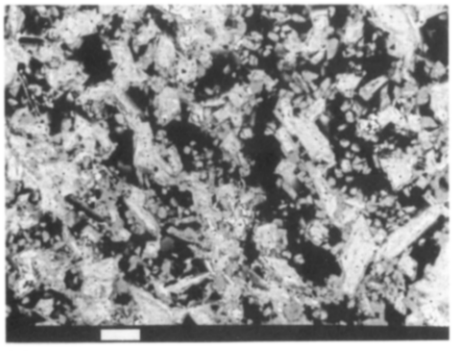

(a)

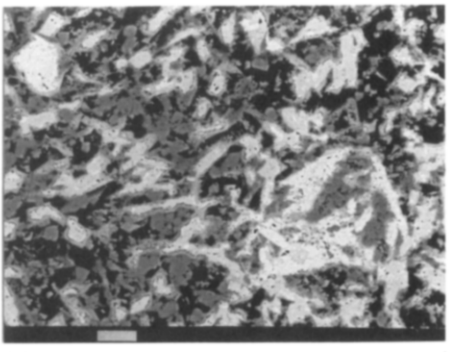

(b)

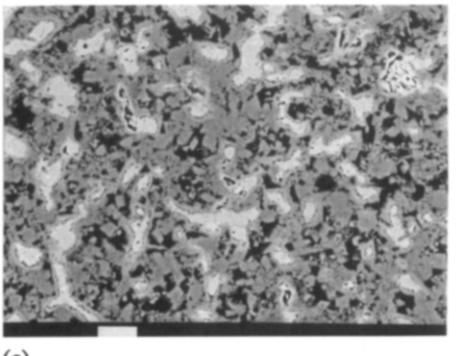

(c)

Fig. 6. Electron micrographs showing progressive growth of sulfation layer around 4BS crystals with soaking time: (a) 6 h; (b) 19 h; (c) 36 h. Magnification bar = 10 μm.

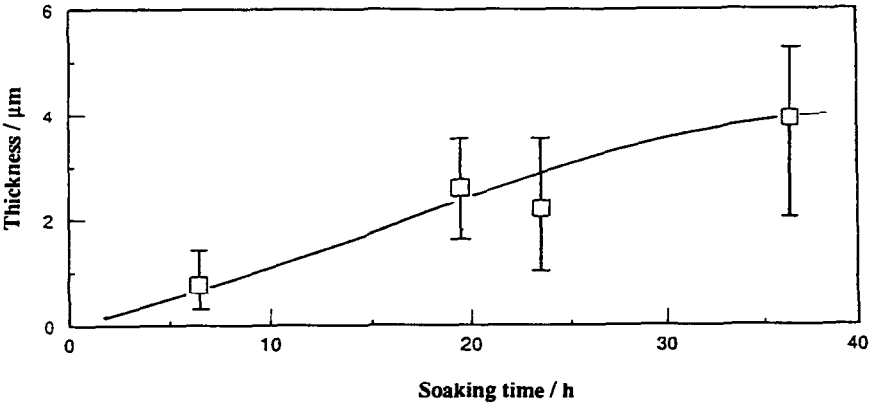

Fig. 7. Development of sulfation layer with soaking time.

washed successively with distilled water and acetone, air dried, and placed in the X-ray diffractometer for phase analysis.

The XRD patterns for both the precursor cured material and a typical example of the resulting oxidation product are given in Fig. 4. The latter comprises a large

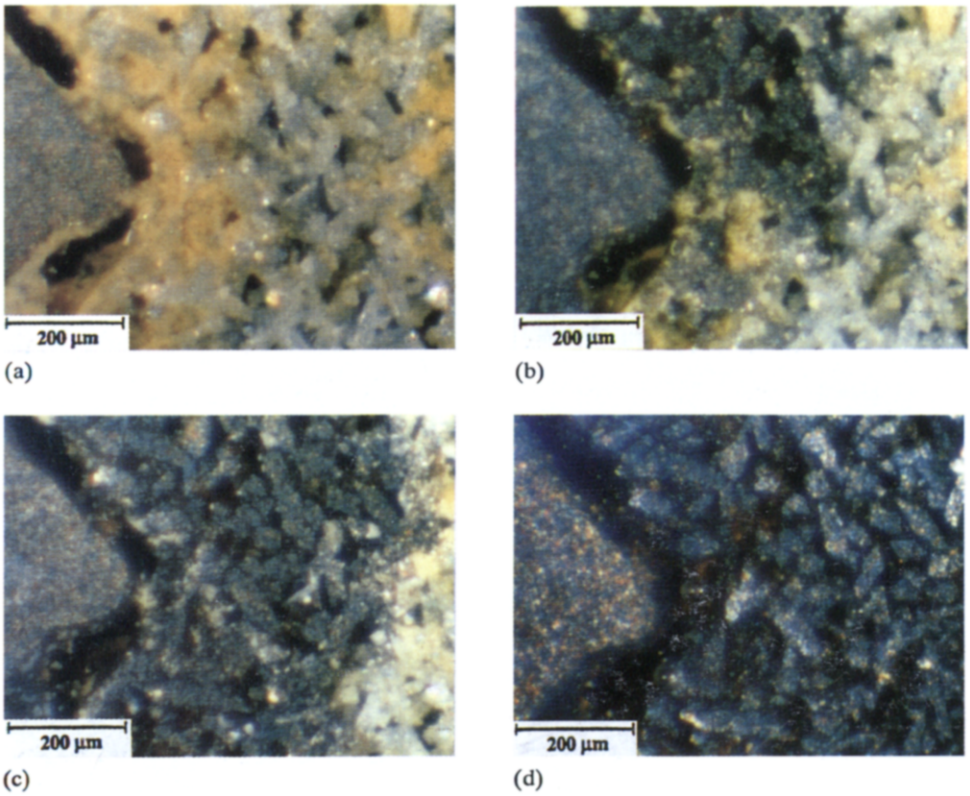

Fig. 8. Optical micrographs of the progressive change in the morphology of cured material during formation at 1.2 V. Magnification: ×78.

amount of β-PbO_2, together with small quantities of both α-PbO_2 and unreacted α-/β-PbO (Fig. 4(b)). The presence of $PbSO_4$ was not detected. The broad peak between 9 and 23° 2θ is due to the amorphous material of the epoxy resin. According to Pavlov *et al.* [18, 34–36], incomplete oxidation of cured material results in either a mixture of α-/β-PbO, 4BS, $PbSO_4$ and α-/β-PbO_2, or a mixture of $PbSO_4$ and α-/β-PbO_2. Therefore, the absence of $PbSO_4$ in this study suggests that complete formation had taken place on the surface of the sample. The detection of α-PbO and β-PbO is probably due to penetration of X-rays through large pores and/or thinner sections of the oxidation product. (Note, the penetration depth of X-rays is usually ~10 μm and is determined by the density and the X-ray adsorption characteristics of the material under study.) Therefore, only the peak heights of β-PbO_2 (and α-PbO_2, if present) were used in determining the composition of the material; the results are presented in Fig. 5. It can be seen that the level of β-PbO_2 increases slightly when the formation potential is raised from 1.1 to 1.15 V and then maintains an approximately constant value of 95 wt.% for potentials up to 1.4 V. Over the corresponding potential ranges, the α-PbO_2 content decreases slightly from 10 to 5 wt.% and then remains unchanged. The cured material undergoes volume changes during oxidation and these create cracks/pores that allow the progressive ingress of acid into the interior of the sample (note, cross-sectional analysis revealed that, in places, the reaction had penetrated

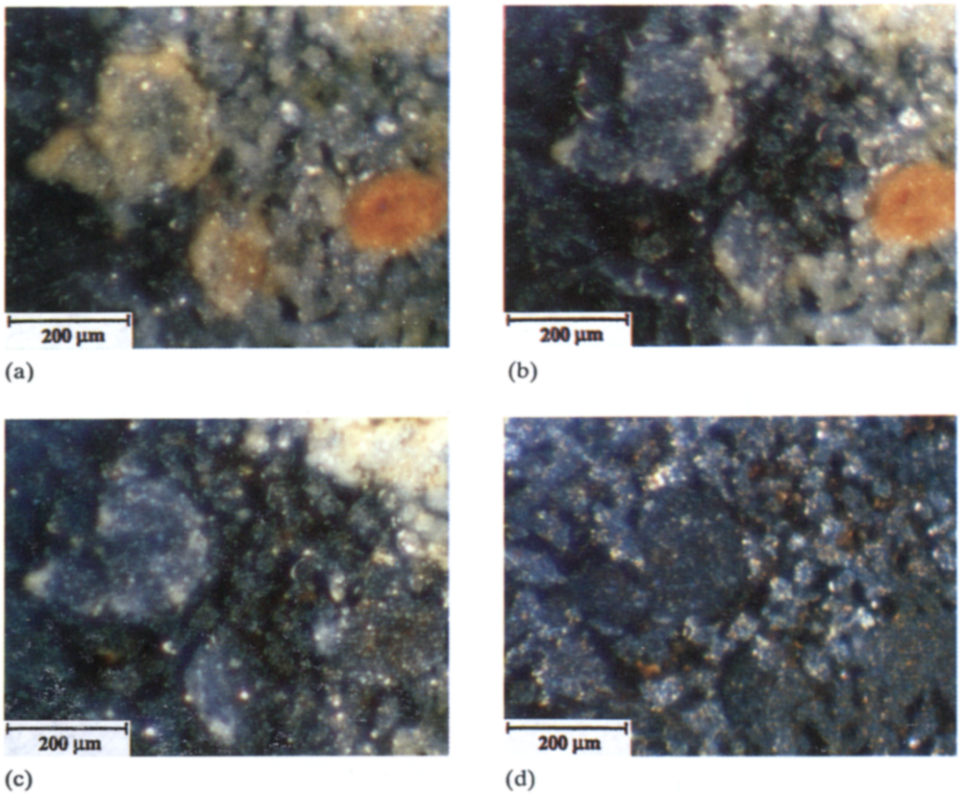

Fig. 9. Optical micrographs of the progressive change in the morphology of cured material during formation at 1.2 V. Magnification: ×78.

to a depth of ~200 μm). Thus, the development of some change in local pH is unavoidable and will account for the appearance of the trace amounts of α-PbO_2. The data given in Fig. 5 therefore confirm that the anodic peak observed at ~1.2 V in the cyclic voltammogram is associated with the formation of β-PbO_2.

Electron micrographs (Fig. 6) clearly show that soaking cured plates in sulfuric acid causes the PbO and 4BS crystals to become covered with a dense film of $PbSO_4$ (dark-grey regions in Fig. 6(a)–(c)). The thickness of the film increases with the soaking time (Fig. 7). After 36 h, all but the largest of the 4BS crystals are converted completely to $PbSO_4$ (Fig. 6(c)). Thus, although cured material may contain different types of basic lead sulfates, the oxidation reaction during plate formation takes place on the same starting material, i.e., $PbSO_4$. Furthermore, it is indisputable that $PbSO_4$ converts to β-PbO_2 during this plate-processing stage. Overall, these findings indicate that the phase composition of cured material exerts little influence on the relative proportions of α- and β-PbO_2 produced during the subsequent formation procedure. Burbank [22] reached a similar conclusion from studies on the constant-current formation of plates prepared from synthetic monobasic, tribasic or tetrabasic lead sulfate.

Formation process

The progress of the formation of 4BS cured material in 1.05 sp. gr. H_2SO_4 was monitored through an optical microscope. Figure 8(a) shows the interface between

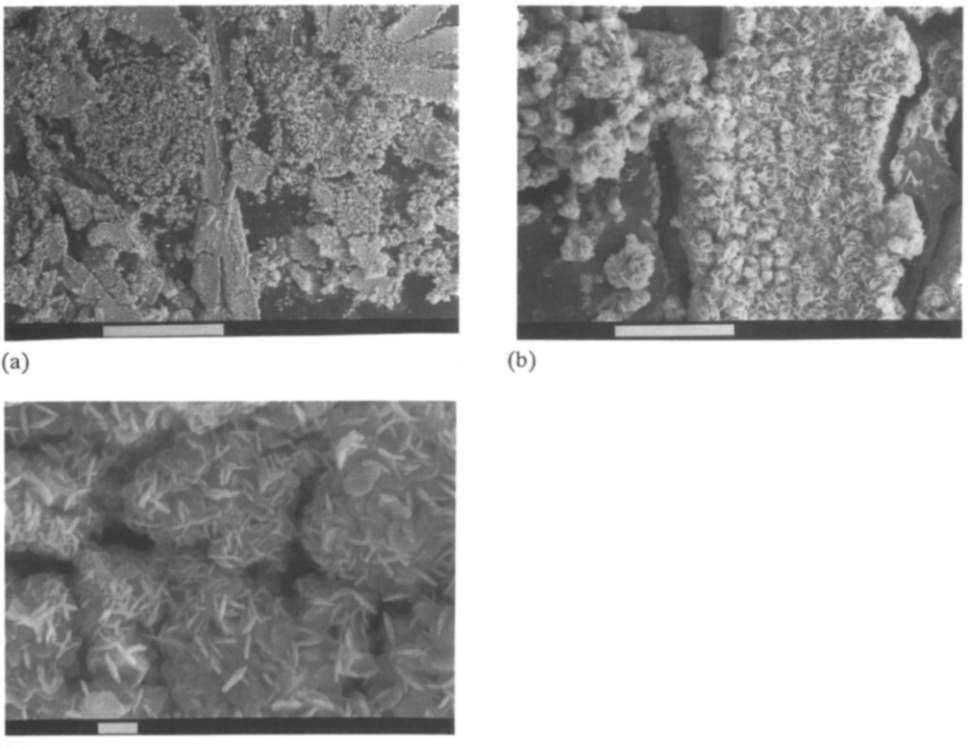

Fig. 10. Electron micrographs of active material formed at 1.1 V. Magnification bar: (a) 100 μm; (b) 10 μm; (c) 1 μm.

the grid and the plate material. The large blue–grey crystals are 4BS. Voids exist between the grid and the cured material and thus the two components are not in complete contact with each other. On application of a constant potential, oxidation commences at the grid surface (by virtue of the metal's high conductivity) and then spreads gradually out into the sample via contact points between the cured material and the grid (Fig. 8(b)). Formation proceeds preferentially along the surface of the 4BS network (Fig. 8(c)) and continues until the entire structure is converted to oxidation product (Fig. 8(d)). Similar phenomena have been examined by Pierson [27].

Figure 9(a) shows a region of cured material that contains 4BS crystals in a matrix of fine leady-oxide particles, together with a red–orange zone of red lead, Pb_3O_4. Again, formation is favoured on the surface of the inter-connected 4BS crystals; the reaction rate is appreciably slower on the isolated, smaller particles of PbO (Fig. 9(b)). In contrast to the latter observation, the oxidation of red lead is rapid (Fig. 9(c) and (d)). Note, it is for this reason that red lead is added to battery plates – especially tubular designs – to increase the efficiency of the formation process. During soaking, the red lead decomposes according to [37]:

$$Pb_3O_4 + 2H_2SO_4 \longrightarrow 2PbSO_4 + \beta\text{-}PbO_2 + 2H_2O \quad (1)$$

The β-PbO_2 acts as a conductive network in the plate material and, thereby, assists the plate formation process.

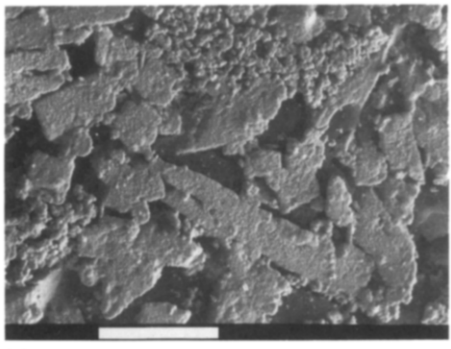

(a)

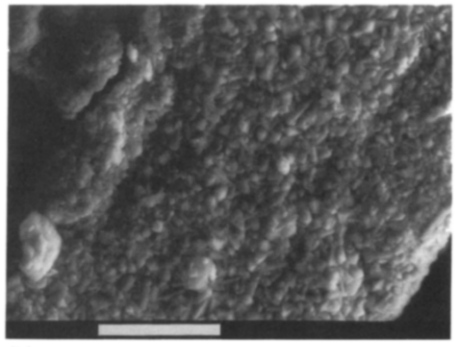

(b)

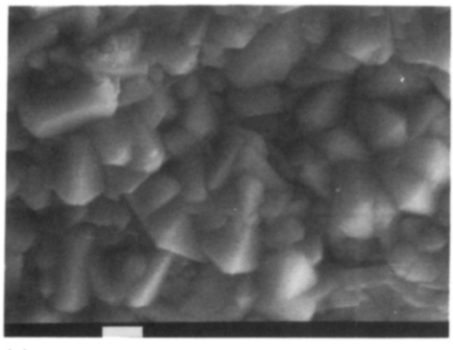

(c)

Fig. 11. Electron micrographs of active material formed at 1.15 V. Magnification bar: (a) 100 μm; (b) 10 μm; (c) 1 μm.

Morphology of formed material

The morphology of the active material produced at different constant potentials from 1.1 to 1.4 V is presented in the form of electron micrographs in Figs. 10–14, respectively. For potentials in the range 1.1 to 1.3 V, the macrostructure appears to follow the shape of the 4BS starting material (cf., Figs. 10(a), 11(a), 12(a) and 13(a)). At 1.4 V, however, vigorous evolution of oxygen occurs and this causes the collapse and disintegration of many of the large 4BS crystals (Fig. 14(a)).

When formation is conducted at 1.1 V, the microstructure is made up of aggregates of individual, plate-like, β-PbO_2 crystals that reside on the surface of the 4BS substrate and are separated by micropores (Fig. 10(b) and (c)). The β-PbO_2 experiences a marked change in morphology when the potential is increased to 1.15 V (Fig. 11(b) and (c)); the crystals are larger, well-defined, and equi-axial or slightly elongated in shape. Nodules of inter-penetrating, flattened and smaller PbO_2 crystals are produced at 1.2 V (Fig. 12(b) and (c)). Increase in the formation potential to 1.3 V results in a further decrease in the size of the crystals together with rounding of their edges and corners to produce anhedral particles that are gathered into 'cauliflower' aggregates (Fig. 13(b) and (c)). The continuous reduction in crystallite size accompanying the rise in formation potential from 1.15 to 1.3 V is in accordance with nucleation/growth theory, i.e., the nucleation rate increases with overpotential. It should be noted, however, that oxygen begins to evolve at 1.3 V and that nascent oxygen species may adsorb at

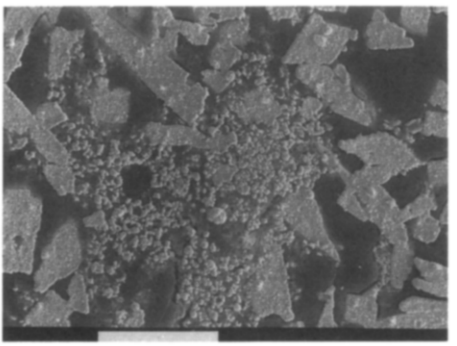

(a)

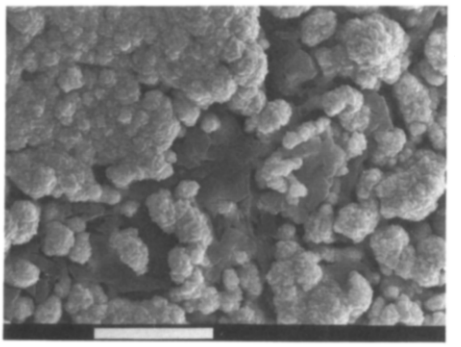

(b)

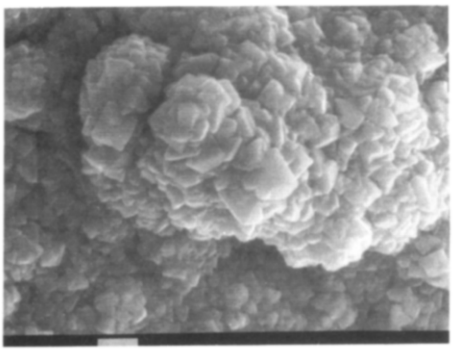

(c)

Fig. 12. Electron micrographs of active material formed at 1.2 V. Magnification bar: (a) 100 μm; (b) 10 μm; (c) 1 μm.

the active sites (i.e., corners and edges) of the developing PbO_2 crystals and, thereby, promote anhedralization and retard further growth.

When the formation potential is raised into the region of vigorous gassing, i.e., 1.4 V, the 4BS crystals are broken up into irregular-sized fragments (Fig. 14(a)). Unlike the microstructures observed above at lower applied potentials, the formed material now consists of different shapes and sizes of β-PbO_2 crystals (Fig. 14(b) and (c)) that are only loosely interconnected. This implies that the intrinsic high mechanical strength of 4BS cured plates is destroyed under overcharge conditions. Indeed, other studies in the CSIRO laboratories have shown that 4BS cured positive plates fail after only 3 or 4 cycles of the reserve capacity test in which, after each discharge, plates are fully recharged at a constant current until the terminal voltage ($\sim$2.7 V/cell) and acid density become constant over three, consecutive, one-hourly readings.

From the above observations, it can be seen that the morphology of the formed material is modified by a change in the applied potential. Given this dependence, PbO_2 crystals of differing size and shape will develop in battery plates formed under constant-current conditions. This, in turn, may partly account for the variability in initial capacity that is often observed with mass-produced batteries. Manufacturers tend to favour a constant-current formation procedure as this is easy to implement and allows an accurate measure of the charge given to the batteries. Nevertheless, the obvious advantages of producing plates with reproducible and controlled morphology

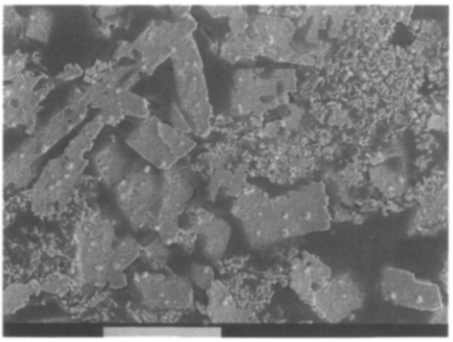

(a)

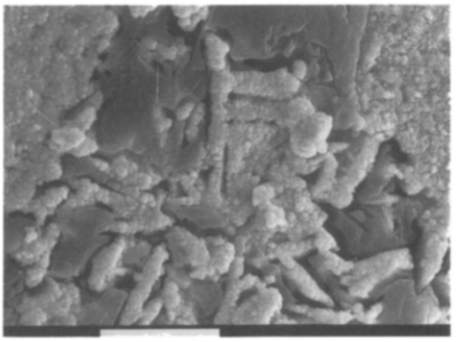

(b)

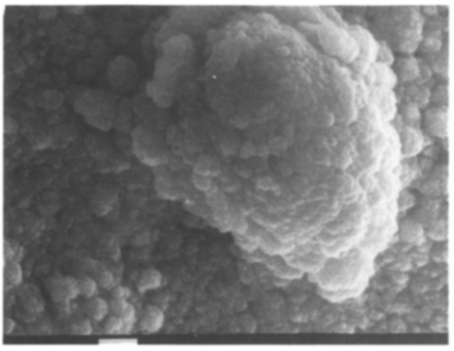

(c)

Fig. 13. Electron micrographs of active material formed at 1.3 V. Magnification bar: (a) 100 μm; (b) 10 μm; (c) 1 μm.

suggests that the alternative technique of constant-potential formation is worthy of consideration.

Conclusions

The objective of this study has been to examine the behaviour of 4BS cured material during the formation of lead/acid battery plates. Battery manufacturers require such information in order to optimize processing conditions and to determine the extent of the benefits to be gained by following the 4BS route for plate production.

An important observation resulting from this work is that the surface of 4BS crystals is chemically converted to a dense layer of $PbSO_4$ that, in turn, is electrochemically oxidized to β-PbO_2 during the subsequent formation stage. This refutes the industry folklore that 4BS is converted preferentially to α-PbO_2. The formation process takes place more readily on the surface of the 4BS network than in regions of unreacted leady oxide.

The morphology of the formed material is strongly influenced by the applied potential. As the latter is raised to more positive values, the PbO_2 structure changes from laminar to anhedral. Formation at high potentials, under vigorous gassing conditions, causes severe attack of the 4BS reticular network and, therefore, may remove the

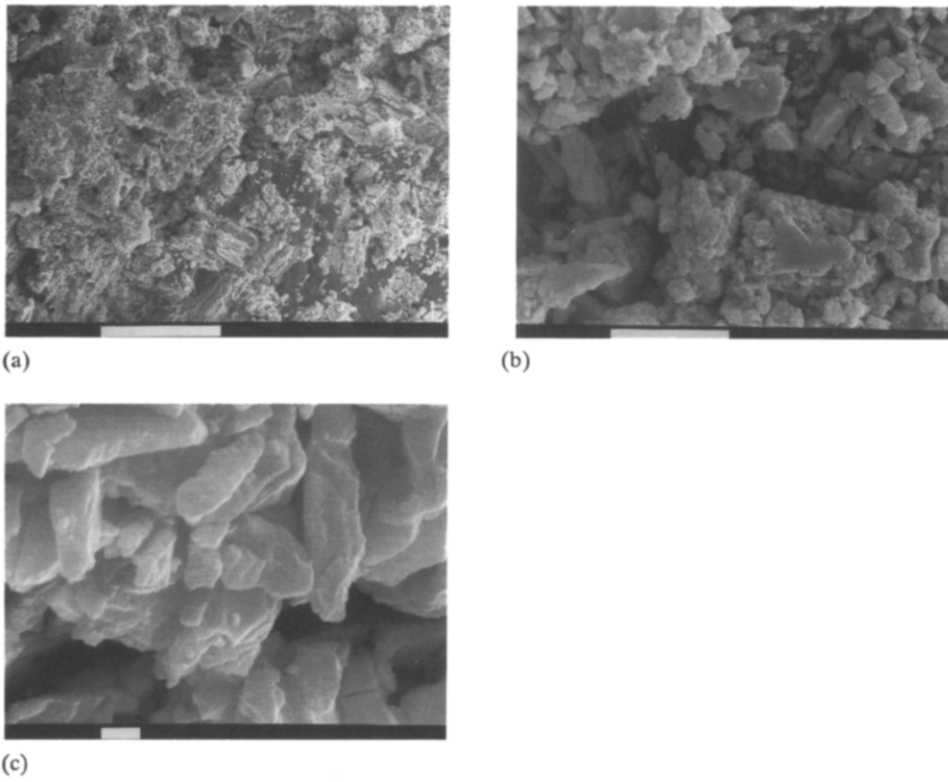

Fig. 14. Electron micrographs of active material formed at 1.4 V. Magnification bar: (a) 100 μm; (b) 10 μm; (c) 1μm.

advantage of greater resilience to deep-discharge cycling that is generally achieved with plates that are cured under high-temperature (4BS) conditions.

References

1 *Lead Chemicals*, International Lead Zinc Research Organization, Inc., New York, 1975, p. 64.
2 B. A. Sexton, G. F. Cotterill, S. Fletcher and M. D. Horne, *J. Vac. Sci. Technol. A, 8* (1990) 544.
3 P. Rüetschi, J. Sklarchuk and P. T. Angstadt, *Electrochim. Acta, 8* (1963) 333.
4 D. A. J. Rand, P. B. Harmer, R. J. Hill and J. A. Wunderlich, in T. Tran and M. Skyllas-Kazacos (eds.), *Electrochemistry: Current and Potential Applications, Proc. 7th Australian Electrochemistry Conf. (7AEC), Sydney, Australia, Feb. 15–19, 1988,* Royal Australian Chemical Institute, Melbourne, 1988, p. 20.
5 V. H. Dodson, *J. Electrochem. Soc., 108* (1961) 406.
6 E. Voss and J. Freundlich, in D. H. Collins (ed.), *Batteries: Research and Development in Non-Mechanical Electrical Power Sources,* Pergamon, Oxford, UK, 1963, p. 73.
7 K. Fuchida, K. Okada, S. Hattori, M. Kono, M. Yamane, T. Takayama, J. Yamashita and Y. Nakayama, *ILZRO Project No. LE-276, Prog. Rep. for 1 January 1978 to 31 December, 1981,* International Lead Zinc Research Organization, Inc., Research Triangle Park, NC, USA, Mar. 31, 1982.

8 W. C. M. Carey, X-ray diffraction as a technique for studying lead-acid battery plates, *Rep. C. R. 21,* July 1965, British Railways Research Department, Derby, UK.
9 N. E. Bagshaw and K. P. Wilson, *Electrochim. Acta, 10* (1965) 867.
10 I. Dugdale, in D. H. Collins (ed.), *Power Sources 1966: Research and Development in Non-Mechanical Electrical Power Sources,* Pergamon, Oxford, UK, 1967, p. 142.
11 W. A. Butler, C. J. Venuto and D. V. Wisler, *J. Electrochem. Soc., 117* (1970) 1339.
12 J. Armstrong, I. Dugdale and W. J. McCusker, in D. H. Collins (ed.), *Power Sources 1966: Research and Development in Non-Mechanical Electrical Power Sources,* Pergamon, Oxford, UK, 1967, p. 163.
13 K. Harris, R. J. Hill and D. A. J. Rand, *J. Electrochem. Soc., 131* (1984) 474.
14 R. J. Hill, D. A. J. Rand and R. Woods, in L. J. Pearce (ed.), *Power Sources 10: Research and Development in Non-Mechanical Electrical Power Sources,* Paul Press, London, UK, 1985, p. 459.
15 V. H. Dodson, *J. Electrochem. Soc., 108* (1961) 401.
16 A. C. Simon and E. J. Jones, *J. Electrochem. Soc., 109* (1962) 760.
17 P. Rüetschi and R. T. Angstadt, *J. Electrochem. Soc., 111* (1964) 1323.
18 D. Pavlov, G. Papazov and V. Iliev, *J. Electrochem. Soc., 119* (1972) 8.
19 S. Ikari, S. Yoshizawa and S. Okada, *Denki Kagaku, 27* (1959) 487; *J. Electrochem. Soc. Jpn., Overseas Ed., 27* (1957) E-186.
20 B. Culpin, *J. Power Sources, 25* (1989) 305.
21 D. Pavlov and G. Papazov, *Electrochemical Power Sources First Symp., E.P.S. Dum Techniky Praha,* 1975, p. 49.
22 J. Burbank, *J. Electrochem. Soc., 113* (1966) 10.
23 R. V. Biagetti and M. C. Weeks, *Bell System Tech. J.,* (Sept.) (1970) 1305.
24 C. F. Yarnell and M. C. Weeks, *J. Electrochem. Soc., 126* (1979) 7.
25 E. J. Taylor, G. A. Shia and D. T. Peters, *J. Electrochem. Soc., 131* (1984) 483.
26 A. C. Simon, in D. H. Collins (ed.), *Batteries 2: Research and Development in Non-Mechanical Electrical Power Sources,* Pergamon, Oxford, UK, 1965, p. 63.
27 J. R. Pierson, *Electrochem. Technol., 5* (1967) 323.
28 R. J. Hill, A. M. Foxworthy and R. J. White, *J. Power Sources, 32* (1990) 315.
29 D. Pavlov and G. Papazov, *J. Appl. Electrochem., 6* (1976) 339.
30 W. Visscher, *J. Power Sources, 1* (1976/77) 257.
31 T. G. C. Chang, M. M. Wright and E. M. L. Valeriote, in D. H. Collins (ed.), *Power Sources 6: Research and Development in Non-Mechanical Electrical Power Sources,* Academic Press, London, UK, 1977, p. 69.
32 A. Komaki, G. Kawamura and S. Mochizuki, *Prog. Batteries Solar Cells, 4* (1982) 167.
33 K. Takahasi, N. Hoshihara, H. Yasuda, T. Ishii and H. Jimbo, *J. Power Sources, 30* (1990) 23.
34 D. Pavlov and G. Papazov, *J. Electrochem. Soc., 127* (1980) 2104.
35 D. Pavlov, *Proc. Symp. Batteries for Traction and Propulsion, Mar. 7–8, 1972,* Columbus Section of the Electrochem. Soc., 1972, p. 135.
36 D. Pavlov, E. Bashtavelova, D. Simonsson and P. Ekdunge, *J. Power Sources, 30* (1990) 77.
37 D. Pavlov and N. Kapkov, *J. Power Sources, 31* (1990) 189.